Journal of The
Electrochemical Society

OPEN ACCESS

Editors' Choice—The Photoelectrochemical and Photocatalytic Properties of Tantalum Oxide and Tantalum Nitride

To cite this article: Vijay Khanal *et al* 2019 *J. Electrochem. Soc.* **166** H3294

View the article online for updates and enhancements.

You may also like

- Photoelectrochemical study of Ta_3N_5 nanotubes for water splitting
Sherdil Khan, Marcos J Leite Santos, Jairton Dupont et al.
- Characterization of Tantalum Nitride Thin Films Deposited on SiO_2 Si Substrates Using dc Magnetron Sputtering for Thin Film Resistors
Nguyen Duy Cuong, Dong-Jin Kim, Byoung-Don Kang et al.
- Synthesis and Photocatalytic Properties of Tantalum Nitride with an Inverse Opal Structure
Toshihiro Moriga, Ai Fujisaka, Natsumi Hirayama et al.

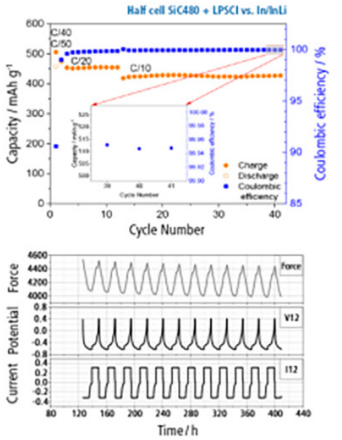
The New PAT-Cell-Solid!

EL-CELL®
electrochemical test equipment

Cycle Solid-State Batteries Under Controlled Pressure of up to 300 MPa (6 mm Diameter)!



- Adjust and measure a force of up to 9000 N on the cell stack!
Force adjustment possible throughout the entire experiment
- Built-in force, and temperature sensors!
With optional gas pressure sensor and gas in- and outlet
- PAT-Solid-Core for easy assembly and reproducible results!
Press and cycle solid-state batteries with 6 or 10 mm electrode diameter
- Cableless and highly sealed battery test cell!
For precise long-term measurements of solid-state cell chemistries



Learn more on our product website:
Scan me!

Download the data sheet (PDF):
Scan me!

Or contact us directly:
+49 40 79012-734
sales@el-cell.com
www.el-cell.com

This content was downloaded from IP address 134.30.220.197 on 15/08/2026 at 04:14

JES Focus Issue on Semiconductor Electrochemistry and Photoelectrochemistry in Honor of Krishnan Rajeshwar

The Photoelectrochemical and Photocatalytic Properties of Tantalum Oxide and Tantalum Nitride

Vijay Khanal,[1] Rowshanak Irani,[2] Sebastian Fiechter,[2] Fatwa F. Abdi,[2] and Vaidyanathan (Ravi) Subramanian[1,2,z]

[1]*Chemical and Materials Engineering, University of Nevada, Reno, Nevada 89557, USA*
[2]*Institute for Solar Fuels, Helmholtz-Zentrum Berlin für Materialien und Energie GmbH, 14109 Berlin, Germany*

The surfactant-assisted synthesis of tantalum oxide nanoparticles (Ta_2O_5), its subsequent nitridation to form tantalum nitride (Ta_3N_5), and the evaluation of the photoactivity of these nanoparticles, are presented. The surface, optical, and compositional characterization of the in-house synthesized photocatalysts indicate spherical nanoparticles with $\phi = 30$ nm Ta_2O_5 and $\phi = 30$ nm Ta_3N_5 with the latter photocatalysts showing absorbance onset at ~ 630 nm. Photoelectrochemical analysis of the various photocatalyst films using chronoamperometry, linear sweep voltammetry, and impedance measurements attribute an improved photoactivity with the *in-house* catalysts to better charge generation, transport, and utilization. Initial results using Ta_2O_5 and Ta_3N_5 demonstrate photocatalytic activity toward conversion of colored pollutants.

© The Author(s) 2019. Published by ECS. This is an open access article distributed under the terms of the Creative Commons Attribution 4.0 License (CC BY, http://creativecommons.org/licenses/by/4.0/), which permits unrestricted reuse of the work in any medium, provided the original work is properly cited. [DOI: 10.1149/2.0391905jes]

Manuscript submitted December 3, 2018; revised manuscript received March 4, 2019. Published March 29, 2019. *This paper is part of the JES Focus Issue on Semiconductor Electrochemistry and Photoelectrochemistry in Honor of Krishnan Rajeshwar.*

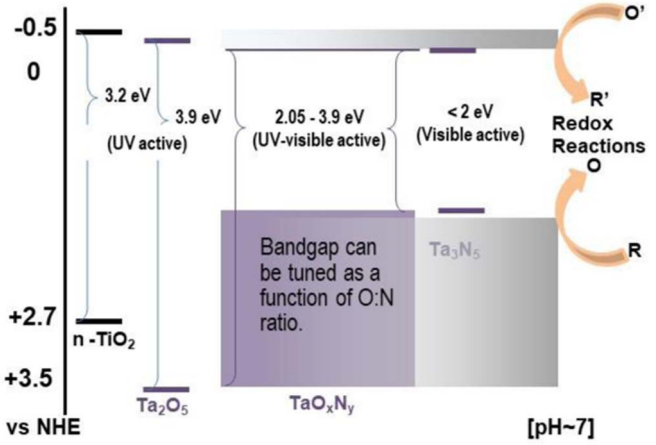
Oxide nanoparticles with single cations have traditionally been used in solar energy transformation. Processes such as photoelectrochemical water splitting or photoelectrochemical remediation of environment are leading examples of solar energy utilization.[1–5] Oxides may be employed i) independently, ii) in combination with another material such as metal or oxide, iii) or in a physically modified manner (such as 0-D or 1-D geometry aka nanoparticles or nanorods). Improving the light absorbance using doping or by using overlying additives is often used for oxides that only absorb in the UV. Popular single metal large bandgap oxides such as TiO_2 or ZnO and formation of their composites with metals,[6] an additional oxide,[7] or chalcogenides[8] demonstrate reasonable photoactivity. However, formation of such composites can often lead to instability driven by phase separation or oxidation of non-oxides.

The multifunctionality of tantalum-based single metal oxides is evident in its dielectric properties,[9] light activated processes,[10,11] and transportation (waveguides).[12] However, tantalum oxides demonstrate very limited photoactivity attributable to its large bandgap (3.6–3.9 eV) which makes it photoactive only in the far right of the UV. However, this large bandgap of tantalum oxide works to our advantage since the bandedges straddle the redox potential of water. This feature makes tantalum oxides a viable candidate, if properly optimized to absorb visible light. For example tantalum oxides may be integrated with the most earth abundant and eco-friendly element – nitrogen – to form oxynitrides – TaO_xN_y [y = 1-x].[13] This singular option allows for tuning the optical bandgap (E_g) over a range of 1.6–4.0 eV n solely based on Ta: O: N ratio n overarching a majority of the visible domain using eco-friendly elements as building blocks. As shown in Scheme 1, such phases are capable of visible light-driven photoactivity.

The synthesis and application of tantalum-based oxides, oxynitrides, and their composites have been reported previously in the literature. However the photoelectrochemical properties and ensuing photocatalytic properties of similarly synthesized materials are not fully understood, especially those that evolve in polycrystalline domain. The tantalum oxides discussed in this work are similar in phase to those reported earlier.[14–16] The application of un-doped and doped tantalum oxides can be noted in the area of water decomposition/hydrogen evolution.[17–19] Furthermore, environmental applications such as photocatalytic oxidation of dyes has also been observed.[16,20,21] Following complete nitridation of the Ta_2O_5 results in the formation of Ta_3N_5 which has been reported to aid with water oxidation/oxygen evolution.[19,22–24] Further, from a greenhouse gas mitigation standpoint, Ta_2O_5 is also reported to aid with CO_2 reduction.[25] Just as with other oxides, the photoactivity of tantalum-based oxides are critically influenced by the method used to synthesize them including the additives used in the synthesis and the shape in which they may evolve.[26,27] This work presents the properties of a surfactant-mediated synthesized Ta_2O_5 nanoparticles with high surface area and specifically examines its surface, optical, and photoelectrochemical features. The practical viability of the nanoparticles is also tested by using it as a photocatalyst for environmental applications.

Experimental

Chemicals.—Tantalum(V) ethoxide (339113-100G, 99.98%, Sigma Aldrich), Tantalum(V) Oxide(Commercial, 88317, 99%, Alfa Products), dry ethanol (V1016, 200 Proof, KOPTEC), Pluronic(P2443-250G) F-127(Powder, Sigma Aldrich), Acetic Acid(42322-0025, ACROS), Hydrochloric Acid (A144C-212, Fisher Chemical, 12.1 Normal) Methylene Blue(M9140-25G, Sigma Aldrich), Ammonia(Anhydrous UN1005, Air gas) were purchased from commercial vendors as indicated in the brackets. Ultra-high purity water for making the solution was obtained using the Millipore



Scheme 1. The relative positions of the bandedges of the tantalum oxide, oxynitrides (TaO_xN_y), and nitride with respect to titanium dioxide.

[z]E-mail: ravisv@unr.edu

water purification system. The chemicals were used "as is" without any alteration or purification for the purpose of synthesis.

Synthesis approach.—The in-house oxide phase was synthesized by implementing the sol-gel process. A typical synthesis involves the use of 2.5g Pluronic(F-127) added with 30ml dry ethanol. The mixture was stirred until the solute was partially solubilized (∼5 minutes). 2.5 ml of glacial acetic acid was added to this solution followed by a dropwise addition of 1 ml HCl. The mixture was ultrasonicated for 3 minutes. Then the solution was magnetically stirred for 15 minutes to add 3ml of Tantalum ethoxide dropwise and then again stirred vigorously for 90 minutes. Finally, the solution was kept at 40°C in air for 15 hours for allowing the gelation process to occur allowing for the formation of the crystallization precursor. Greenish white grains were recovered and placed in a convective oven at 65°C for 24 hours to burn off the moisture. Subsequently, ramping the temperature up to 700°C over 12 hours slowly burned off the precursor associated carbon content. Fine white crystals (identified as Ta_2O_5 as discussed later) were formed as a result after the oxidative annealing. They were crushed using mortar and pestle to collect in the form of fine shining-white powder.

These crystals of Ta_2O_5 were used as the starting precursor for the synthesis of the nitrides, Ta_3N_5. A representative step involved placing the white crystals in a high temperature furnace to perform nitridation in the presence of a continuous ammonia flow at 850°C (Ammonia flow Rate ∼1000ml/min). It was noted that the ammonia flowrate affected the coloration of the final product. For photoelectrochemical measurements, the powdered samples of Ta_2O_5 (or Ta_3N_5) were mixed thoroughly with terpinol and made as fine slurry suspension. 0.1g of photocatalyst was taken in a glass vial, mixed with 0.2 ml of terpinol, and magnetically stirred for 30 minutes. Single drop of thus obtained slurry was casted on ∼ $2/3^{rd}$ of the length of the ITO coated glass slides (ITO coated glass plates were obtained from Pilkington Ford, OH) using 1 ml plastic pipette, and the slide was slanted (∼ 15^0 angle) so that the slurry self-transforms into a uniform film by flowing under gravity. These ITO slides were dried at ∼80°C for 30 minutes and were annealed at 350°C for 4 h under an inert (N_2) atmosphere prior to use in photoelectrochemical measurements.

Material characterization.—The characterization of the photocatalysts was performed using several complementary tools. A Hitachi S-4700 scanning electron microscope (SEM) was used to examine the physical features of the powder. High resolution transmission electron microscopy ((HR)TEM) analysis was performed using a JEOL 2100F instrument equipped with a selected area electron diffraction (SAED) analyzer. The optical properties of the powder were examined using a UV–vis diffuse absorbance measurement with a Shimadzu UV 2501PC spectrophotometer. Brunauer Emmett- Teller specific surface areas (S_{BET}) of the synthesized materials were determined using a micromeritics system. X-ray diffraction patterns were taken using a Bruker D8 diffractometer (Cu Kα radiation, 40 mA, 40 kV). X-ray photoelectron spectroscopy (XPS) measurements were done under a monochromatic Al Kα X-ray source (1486.74 eV, Specs Focus 500 monochromator). The photoelectrons were detected with a hemispherical analyzer (Specs Phoibos 100). The binding energies were calibrated to the adventitious carbon peak.

Determination of photoelectrochemical properties.—The photoelectrochemical measurements were performed using a potentiostat/galvanostat (Autolab PGStat series). The measurements were recorded for films of the photocatalyst prepared by depositing an aqueous suspension of the photocatalyst slurry on conducting (FTO) glass slide followed by N_2 annealing at 350°C. Chronoamperometry, Linear sweep voltammetry, and measurements for bandgap estimation (tauc plots) were obtained using 0.2 M aqueous NaOH. A Xe lamp was used as a light source with a $CuSO_4$ filter for high UV cut off. A Pt mesh was used as the counter electrode and Ag/AgCl was used as a reference [Filling Electrolyte(In the reference electrode): 3.4M KCl, electrolyte used: 0.2M NaOH].

Determination of photocatalytic properties.—For photocatalysis studies, a suspension of the synthesized material was prepared with various dyes independently in water. Ta_2O_5 or Ta_3N_5 and 200 ml of 28.6 μM Methylene Blue solution or 28.6μM Rhodamine B solution, under aerated conditions were used. The sample solution was sonicated for 3 minutes before it was transferred to a jacketed borosilicate reactor and was left in dark for 1.5 hours under constant magnetic stirring so as to achieve adsorption-desorption equilibration. Then the solution was illuminated using a 480 W solar simulator lamp from the top for determining the activity of the materials as a photocatalyst. The change in concentration of the dyes upon illumination (and hence the photoactivity of the catalyst samples) was tracked by sampling 3 ml of the solution every 30 minutes for four times (total illumination period: 2 hours), centrifuging it, and eventually measuring the optical absorbance with UV-vis spectrophotometer. The absorbance data was then corresponded with instantaneous concentration of the dye based upon Beer-Lambert's law.

Results and Discussion

Characterization of the photocatalyst.—*Analysis of nanoparticle morphology using SEM.*—The size and shape of the procured and synthesized oxides were initially examined using microscopy. As evident from the Figure 1a, the commercial samples are non-spherical with nanoparticles starting at 40 nm. There are clusters consisting of 3–4 aggregated nanoparticles that are ∼100–150 nm observed. The SEM image of the in-house synthesized after thermal treatment is shown in Figure 1b. In comparison, the size distribution among the in-house nanoparticles is narrow and well controlled. These nanoparticles appear more spherical with distinct boundaries and smaller diameter in the range of 20–30 nm. The nanoparticles appear to be better dispersed and do not show evidence of cluster formation. The reductive treatment shows an insignificant impact on the physical features of the oxides. The post treatment (nitridation process) dimensions of the nanoparticles are mostly in the 30 – 40 nm range as indicated in Figure 1c. There is also no evidence of clustering of the nanoparticles. Given this size of the nanoparticles, the approach used to prepare the films using a binder, and the amount of the material taken as a slurry, the particulate films formed is expected to evolve with film thickness upto a few microns.

Physical features and crystallinity of the nanoparticles.—TEM analysis is important because a smaller size of the in-house synthesized samples can be indicative of availability of more surface, which is consistent with a surfactant – assisted method used for synthesis. The TEM and HRTEM analysis of the in-house synthesized thermally annealed samples before and after treatment under ammonia flow is shown in Figure 2A. The thermally annealed samples appear to be ∼6–7 nm while the nitride samples are ∼20–30 nm. All annealed samples show distinct evidence of crystallinity as indicated in the HRTEM. Furthermore, the presence of the geometric diffraction patterns in the SAED confirms thermally induced crystallization. The spacing are marked in the figure and suggest that the samples are Ta_2O_5 and Ta_3N_5. This is further confirmed by their X-ray diffraction patterns, which clearly match those of Ta_2O_5 and Ta_3N_5, respectively as indicated in Figure 2B.

Estimation of the surface area of these nanoparticles (using single point BET measurements) was performed using N_2 physisorption. The estimated values for the commercial Ta_2O_5, (in–house) Ta_2O_5, and Ta_3N_5 are 1.6 m^2/g, 41 m^2/g and 17 m^2/g respectively. The higher surface area is attributed to the smaller nanoparticles and minimal aggregation.

X-ray photoelectron spectroscopy (XPS) measurements were performed in order to investigate the chemical nature of the samples. Core-level spectra for the Ta_2O_5 and Ta_3N_5 samples are shown in Figure 2C. Ta_2O_5 samples only show a peak at 404.9 eV (Ta $4p_{3/2}$), and no

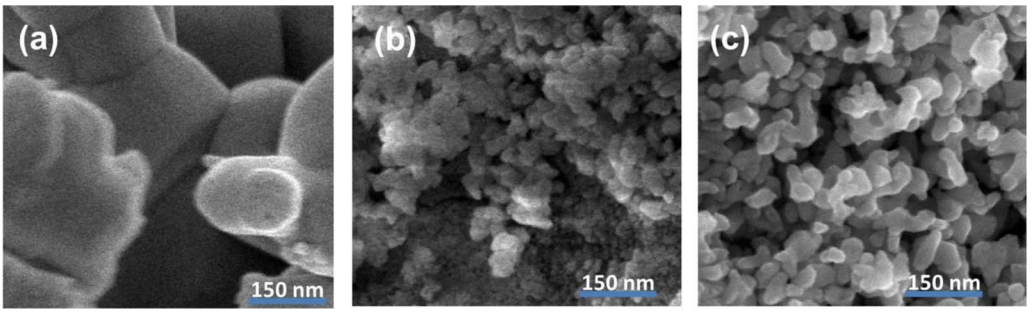


Figure 1. The microscopic images obtained using scanning electron microscope (SEM) of the (a) commercial Ta_2O_5 nanoparticles, in-house thermally annealed oxides (b) before, and (c) after reductive treatment.

peak for nitrogen. The Ta $4p_{3/2}$ peak shifts to lower binding energy for the Ta_3N_5 samples, which is attributed to the lower electronegativity of N as compared to O. In addition, the Ta_3N_5 samples show peaks at binding energies of 396.7 and 394.8 eV, which can be assigned to N 1s.

Optical analysis using spectroscopy.—The nanoparticles were deposited as films on FTO coated glass before determining their optical response. The absorbance spectra of the films are shown in Figure 3a, the Tauc's plots for bandgap estimation are shown in Figure 3b while the Figure 4 shows photographs of the powders prior to their deposition. Both commercial and in-house Ta_2O_5 are white and show an onset absorbance of 320 nm. Ta_2O_5 bandgap are estimated to be in the range of 3.6–3.9 eV based on the onset absorbance and they are consistent with the literature reported observations.[28] This onset is also evidence that the photoactivity is driven predominantly by UV light. The Ta_3N_5 shows a redshift as far as ~630 nm with the onset broadening the absorbance indicative of a much smaller bandgap. The experimental determination of the bandgap was performed using Tauc plot analysis[29,30] A bandgap of 3.66 eV and 1.68 eV for Ta_2O_5 and Ta_3N_5 respectively is estimated as indicated in Figure 3b. (Note that, the approximate and relative bandedge positions are reported based on

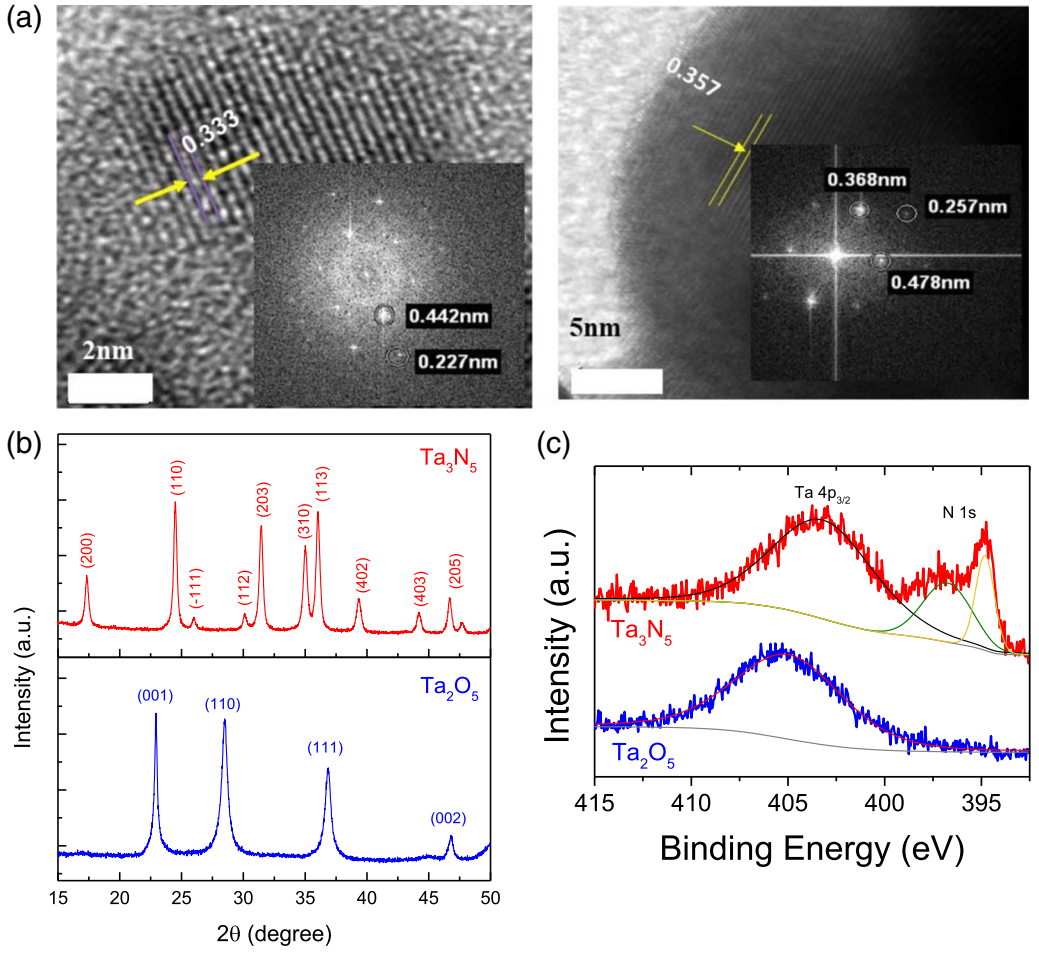


Figure 2. (A) The figure shows the HRTEM images of the in-house synthesized thermally annealed samples (a) before and (b) after treatment in ammonia flow. The insert shows the SAED pattern indicating that the annealed samples are Ta_2O_5 and Ta_3N_5 respectively. (B) The figure shows the X-ray diffraction pattern of the in-house synthesized thermally annealed samples: Ta_3N_5 (top) and Ta_2O_5 (bottom) with the corresponding <hkl> values indicating that the compounds are polycrystalline. (C) Ta $4p_{3/2}$ and N 1s core-level X-ray photoelectron spectra of Ta_2O_5 and Ta_3N_5 nanoparticles.

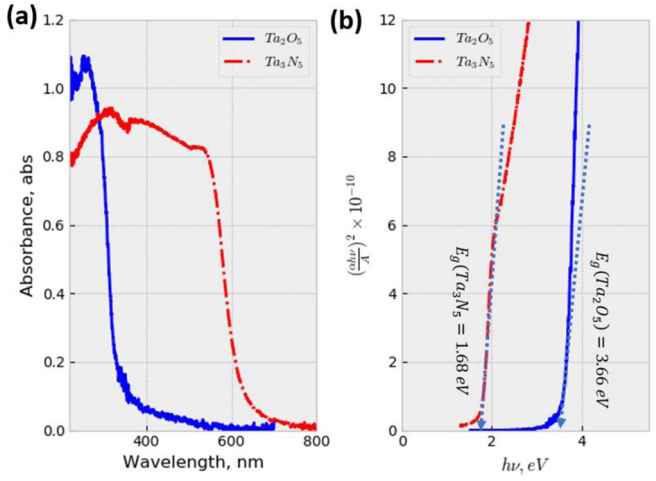


Figure 3. UV-vis absorbance spectra for Ta_2O_5 (as-synthesized, after thermal treatment) and Ta_3N_5 are shown in (a), and corresponding Tauc's plot for bandgap estimation are shown in (b). The Tauc's plot of the in-house synthesized material indicates Ta_2O_5 has bandgap (E_g) = 3.66 eV and for Ta_3N_5, E_g = 1.68 eV.

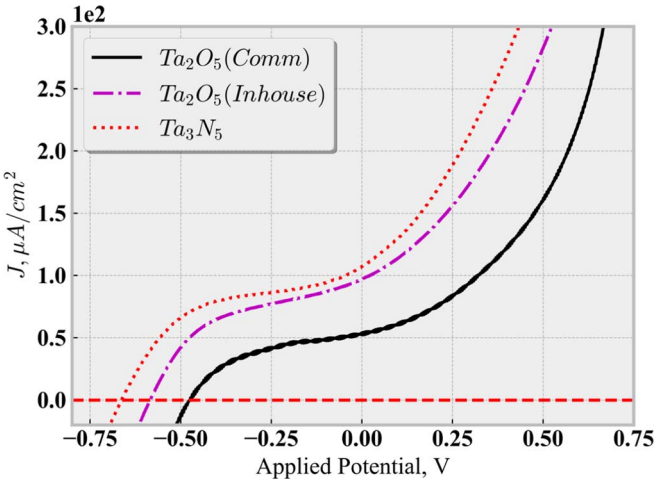


Figure 6. The linear sweep voltammogram (j/V) responses of (a) Ta_3N_5, (b) In-houseTa_2O_5, and (c) commercial Ta_2O_5 is shown. [Operating conditions: Pt counter electrode, leak-free Ag/AgCl (in 0.2M NaOH) as the reference electrode and sample coated ITO slide as working electrode.].

illuminated conditions). The coloration is indicative of the incorporation of nitrogen in the Ta_2O_5. It is to be noted that thermal reduction protocol is applied on Ta_2O_5 for this reason, i.e. to broaden the absorbance response from UV to include visible light.

Chronoamperometry (j/t) and linear sweep voltammetry (j/V) measurements.—The analysis of photoelectrochemical or PEC data offer valuable information into the separation and transport mechanisms of charges photogenerated in the catalysts upon illumination. This approach allows to track both hole and electrons upon generation in the catalysts and can be correlated with the photocatalytic activity.[31,32] The chronoamperometry or j/t responses of the commercial and in-house synthesized Ta_2O_5 obtained with a Pt wire as the counter electrode in a 3-electrode PEC cell are shown in Figures 5a and 5b. The electrolyte was alkaline to facilitate the removal of holes using hydroxyl ions [$OH^- + h^+ \rightarrow OH^\bullet$]. The multiple on-off cycles show that the response in both films are light triggered and the reproducible nature of these responses indicate that the films formed on the conducting glass slides are reproducible. The inset of the Figures 5a and 5b shows the photographs of the films after the PEC measurements, indicating they are stable (do not delaminate). The in-house Ta_2O_5 shows a differential photocurrent (illuminated – dark) of 1.3 $\mu A/cm^2$ while the commercial Ta_2O_5 response is approximately 0.85 $\mu A/cm^2$. This increase in photocurrent by ~50% with the in-house Ta_2O_5 could be attributed to the difference in the physical dimensions of the nanoparticles and/or the improved photoactivity of this film, but has to be verified using alternative approaches (discussed below). At the same time, the corresponding photocurrent using Ta_3N_5 is observed to be 8 $\mu A/cm^2$ ~ 4 times increase in the photoresponse (Figure 5c) compared to the Ta_2O_5. [Note, that the differential (illuminated – dark) current is 4 $\mu A/cm^2$]. This shows that the evolution of the redox charges in the nitride is significantly higher compared to the oxide.

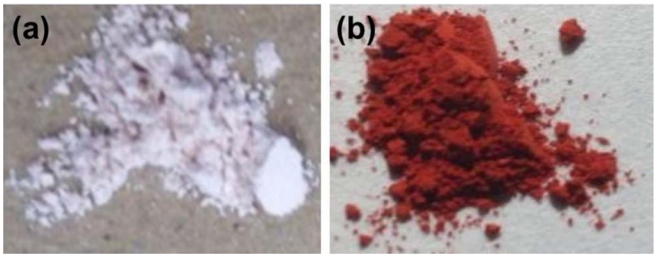


Figure 4. The photographs of the in-house synthesized (a) Ta_2O_5 (annealed) and (b) Ta_3N_5 after nitridation.

The linear sweep voltammogram or j/V plot of the films are shown in Figure 6. Linear sweep voltammogram are different than the current-time (chronoamperometry) characteristics as they provide insight into the relative position of "apparent flatband potentials" for the film and thereby help qualitatively distinguish the charge separation in the films. The magnitude of the photocurrent obtained in the 3-electrode setup is shown to be higher by ~10% with the in-house Ta_2O_5

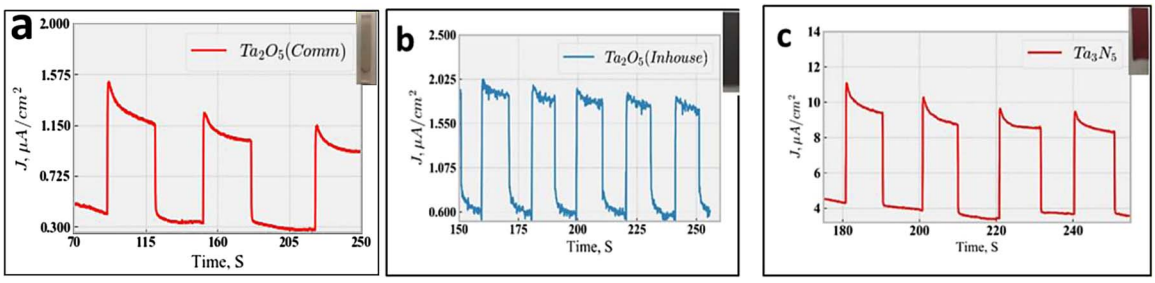


Figure 5. The chronoamperometry (j/t) responses of (a) commercial (b) In-house Ta_2O_5 and (c) Ta_3N_5 illumination. [Operating conditions: Pt counter electrode, leak-free Ag/AgCl (in 0.2M NaOH) as the reference electrode and sample coated ITO slide as working electrode. Light intensity: 80 mW/cm^2, applied potential – no external bias was applied in the three electrode system except the intrinsic potential developed in the film upon illumination, estimated film thickness: ~1–2 μM].

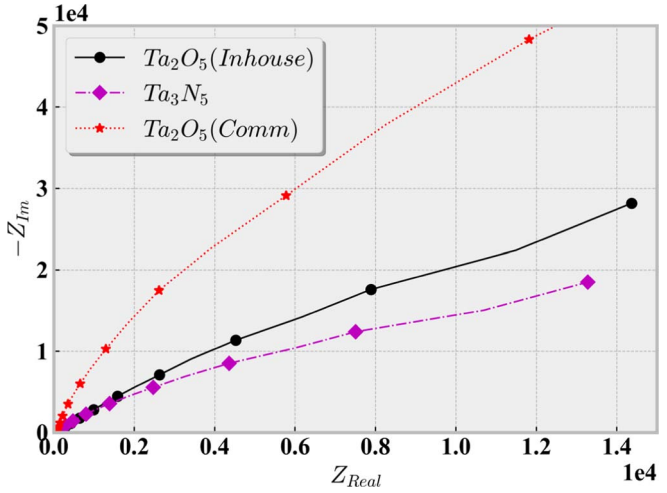


Figure 7. The figure results of the electrochemical impedance analysis (EIS, Nyquist Plots) of (a) commercial Ta_2O_5, (b) in-house Ta_2O_5, and the in-house, and (c)Ta_3N_5 are shown. [Operating conditions: All measurements in illumination by 80 mW/cm^2 Xenon lamp, Pt counter electrode, leak-free Ag/AgCl (in 0.2M NaOH) as the reference electrode and sample coated ITO slide as working electrode.].

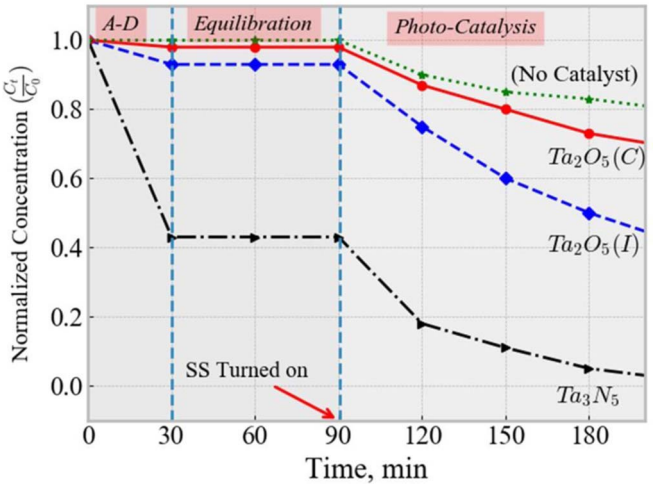


Figure 8. The photodegradation of methylene blue or MB was performed using UV-visible light after 1.5 hours of equilibration under dark to ensure adsorption (A-D). 0.1g of commercial [Ta_2O_5(C)] and in-house synthesized [Ta_2O_5(I) & [Ta_3N_5] were used in the photocatalyst with a solar simulator (SS) as the light source [Light: 480W solar simulator, distance between the reactor and light source: 30cm.].

compared to the commercial equivalent. The zero current potential is a measure of the apparent flatband potential in the film and is often estimated to provide an insight into the band bending in particulate films.[33] A more negative shift is indicative of charges separating effectively and becoming available for transport or redox activity. At −0.57 V and −0.48 V vs. Ag/AgCl the in-house film shows ∼90 mV negative shift and is thus indicative of a better charge separation compared to the commercial Ta_2O_5 respectively. Such responses from well controlled nanoparticulate films of oxides are reported with other oxides such as TiO_2 as well.[33]

Impedance analysis.—The basis for performing the impedance analysis on the tantalum – based photocatalysts is to gain insights into film properties such as the n-/p-characteristics and a qualitative estimate of the extent of charge separation.[34,35] The plot of the impedance response for the Ta_2O_5 and Ta_3N_5 photocatalyst films is shown in Figure 7. The Ta_2O_5 in-house sample shows a low radius of curvature compared to the commercial sample indicating that charge separation is better with the in-house samples. Finally, the application of the nitridation process to Ta_2O_5 to form Ta_3N_5 is beneficial as it shows the lowest radius of curvature indicating the most effective transport among the three photoactive films. Thus, the series of PEC measurements indicate that i) the in-house Ta_2O_5 and Ta_3N_5 demonstrate photocurrent generation, ii) reproducible and stable response, and iii) the Ta_3N_5 demonstrates a distinguishable enhancement in the photocurrent response compared to the Ta_2O_5 films which can be attributed to the better charge separation, transport across the film thickness, and collection at the underlying FTO plate.

Photocatalytic activity.—*Methylene blue absorbance and photolytic conversion.*—Methylene blue (MB) is a multi-purpose organic colored dye used in textile industries and considered a representative model pollutant whose photodegradation can be tracked using spectroscopy to determine the activity of the photocatalyst.[36,37] Rajeshwar and coworkers have extensively studied the photoactivity of MB in the presence of various oxides.[38–40] They have demonstrated that the dye could be degraded in the presence of a photocatalyst with and without an electric field. A simple approach to probe methylene blue degradation is to track the decrease in dye absorbance in the visible. Figure 8 shows the changes to the dye absorbance at 664 nm in the absence and presence of catalysts, since photolytic conversion of MB is reported.[41]

As evident in Figure 8 that MB undergoes photolytic conversion up to 20% over 2 hours of continuous UV-vis illumination.

Comparison of the commercial and in-house Ta_2O_5 photocatalysts.—Figure 8 also shows the change in the absorbance of the dye solution at various time before and after illumination. Compared to the control experiments (catalyst-free conditions) a higher dye conversion is observed attributable to the degradation initiated in the presence of the Ta_2O_5. In the presence of the commercial and in-house Ta_2O_5 a significant decrease in the peak absorbance is observed over a period of 2 hours of continuous illumination. The commercial Ta_2O_5 of 0.1 g loading shows a 31% decrease in the dye concentration. In contrast, the in-house Ta_2O_5 shows a 58% decrease over the same period, with the same loading. Since MB is not regarded as an "ideal pollutant" the activity of the commercial and in-house Ta_2O_5 was further compared toward the degradation of Rhoadamine B (RhB). The degradation of 200 ml 28.6μM RhB, under aerated conditions using a 480 W solar simulator at the end of 3.5 hours (1.5 hour dark + 2 hours illumination) was observed to be 45% and 80% respectively using commercial and in-house Ta_2O_5 suggesting the in-house Ta_2O_5 is far superior. The improvement in the dye degradation with the in-house catalyst can be attributed, to the smaller particle size of the in-house Ta_2O_5 as evident from the SEM and (HR)TEM analyses.

Comparing in-house Ta_2O_5 with in-house Ta_3N_5.—Ta_3N_5 produced by thermal reduction process was tested as a photocatalyst for the degradation of MB. During equilibration, the dark absorbance region is remarkably different for the two photocatalysts. Considering the fact that the Ta_3N_5 are bigger than the Ta_2O_5, interestingly enough a significant drop in absorbance of the dye is noted during dark equilibration with Ta_3N_5. This is indicative of a very effective absorbance of the dye on the Ta_3N_5 surface than the Ta_2O_5. Preliminary estimated of the fractional conversion of the dye using Ta_3N_5 was determined to be ∼90%. One of the noteworthy observations is the high dark adsorption of the MB on the Ta_3N_5. The role of this adsorption in promoting photocatalysis remains to be fully understood.

Conclusions

The synthesis of Ta_2O_5 nanoparticles using a surfactant assisted process and its subsequent complete thermal nitridation to Ta_3N_5

using NH_3 has been demonstrated. The physical features, phase evolution, and optical properties is systematically analyzed and indicates that 30–40 nm diameter nanoparticles with tight size control can be synthesized. The photoelectrochemical measurements of the films prepared on ITO indicates enhanced separation of photogenerated charges attributable to higher surface area and better particle size. With the in-house samples, photocurrent comparing illuminated – dark conditions indicates an increase from 1.3 $\mu A/cm^2$ for Ta_2O_5 to ~4 $\mu A/cm^2$ for Ta_3N_5. The linear sweep voltammetry and impedence analysis clearly indicates the superior performance of the in-house synthesized Ta_2O_5. Preliminary results indicate the both Ta_2O_5 and Ta_3N_5 may be used as a photocatalyst for photo-oxidative reactions with Ta_3N_5 particularly demonstrating promising adsoprtion and photocatalytic activity.

Acknowledgments

The support from the Alexander von Humboldt foundation to R.S.V. is acknowledged. Notable contribution from Cara DuMonte as an undergraduate intern is also acknowledged. The assistance provided by Pawan Pathak and Dr. Mojtaba Ahmedian is gratefully acknowledged.

ORCID

Fatwa F. Abdi https://orcid.org/0000-0001-5631-0620
Vaidyanathan (Ravi) Subramanian
https://orcid.org/0000-0001-9523-3074

References

1. J. R. Bolton, *Solar Energy*, **57**, 37 (1996).
2. K. Drew, G. Girishkumar, K. Vinodgopal, and P. V. Kamat, *J. Phys. Chem. B*, **109**, 11851 (2005).
3. K. Rajeshwar, M. K. Hossain, R. T. Macaluso, C. Janaky, A. Varga, and P. J. Kulesza, *J. Electrochem. Soc.*, **165**, H3192 (2018).
4. W. Chanmanee, N. R. de Tacconi, K. Rajeshwar, W. Y. Lin, L. Nikiel, and W. A. Wampler, *J. Electrochem. Soc.*, **159**, F226 (2012).
5. E. M. Shin, R. Senthurchelvan, J. Munoz, S. Basak, K. Rajeshwar, G. BenglasSmith, and B. C. Howell, *J. Electrochem. Soc.*, **143**, 1562 (1996).
6. S. T. Kochuveedu, Y. H. Jang, and D. H. Kim, *Chemical Society Review*, **42**, 8467 (2013).
7. S. Hernández, V. Cauda, A. Chiodoni, S. Dallorto, A. Sacco, D. Hidalgo, E. Celasco, and C. F. Pirri, *ACS Applied Materials and Interfaces*, **6**, 12153 (2014).
8. P. Pathak, S. Gupta, A. C. S. Resende, and V. Subramanian, *J. Mater. Chem. A*, **3**, 24297 (2015).
9. C. Chaneliere, J. L. Autran, R. A. B. Devine, and B. Balland, *Materials Science & Engineering R-Reports*, **22**, 269 (1998).
10. S. Naveenraj, G. J. Lee, S. Anandan, and J. J. Wu, *Mater. Res. Bull.*, **67**, 20 (2015).
11. E. E. Nikishina, E. N. Lebedeva, and D. V. Drobot, *Inorg. Mater.*, **48**, 1243 (2012).
12. J. M. Mir and J. A. Agostinelli, *Journal of Vacuum Science & Technology A*, **12**, 1439 (1994).
13. C. Ho, K. Low, and P. e. a. Jash, *Chem. Mater.*, **23**, 4721 (2011).
14. V. Vo, N. V. Kim, N. T. V. Nga, N. T. Trung, L. T. Giang, P. V. Hanh, L. H. Hoang, and S. J. Kim, *J. Electron. Mater.*, **45**, 2334 (2016).
15. S. G. Ghugal, S. S. Umare, and R. Sasikala, *RSC Adv.*, **5**, 63393 (2015).
16. C. Tao, L. L. Xu, and J. G. Guan, *Chem. Eng. J.*, **229**, 371 (2013).
17. L. Xu, J. Guan, and W. Shi, *ChemCatChem*, **4**, 1353 (2012).
18. R. V. Goncalves, P. Migowski, H. Wender, D. Eberhardt, D. E. Weibel, F. C. Sonaglio, M. J. M. Zapata, J. DuPont, A. F. Feil, and S. R. Teixeira, *J. Phys. Chem. C*, **116**, 14022 (2012).
19. Y. Luo, X. M. Liu J., X. H. Tang, Y. Luo, Q. Y. Zeng, X. L. Deng, S. L. Ding, and Y. Q. Sun, *J. Mater. Chem. A*, **2**, 14927 (2014).
20. J. C. Rooke, T. Barakat, J. Brunet, Y. Li, M. F. Finol, J. F. Lamonier, J. M. Giraudon, R. Cousin, S. Siffert, and B. L. Su, *Applied Catalysis B: Environmental*, **162**, 300 (2015).
21. H. Q. Sun, S. Z. Liu, S. M. Liu, and S. B. Wang, *Applied Catalysis B-Environmental*, **146**, 162 (2014).
22. S. S. K. Ma and K. H. Maeda, T. et al., *Chemistry A European Journal*, **19**, 7480 (2013).
23. S. S. K. Ma, T. Hisatomi, K. Maeda, Y. Moriya, and K. Domen, *Journal of American Chemical Society* **134**, 19993 (2012).
24. H. X. Dang, N. T. Hahn, H. S. Park, A. J. Bard, and C. B. Mullins, *J. Phys. Chem. C*, **116**, 19225 (2012).
25. S. Sato, T. Morikawa, S. Saeki, T. Kajino, and T. Motohiro, *Angewandte Chemie-International Edition* **49**, 5101 (2010).
26. J. Huang, R. Ma, Y. Ebina, K. Fukuda, K. Takada, and T. Sasaki, *Chem. Mater.*, **22**, 2582 (2010).
27. J. Li, W. Dai, G. Wu, N. Guan, and L. Li, *Catal. Commun.*, **65**, 24 (2015).
28. N. Ndiege, T. Wilhoite, V. Subramanian, M. A. Shannon, and R. I. Masel, *Chem. Mater.*, **19**, 3155 (2007).
29. S. M. Wang, Y. Guan, L. P. Wang, W. Zhao, H. He, J. Xiao, S. G. Yang, and C. Sun, *Applied Catalysis B-Environmental*, **168**, 448 (2015).
30. D. R. Jones, V. Gomez, J. C. Bear, B. Rome, F. Mazzali, J. D. McGettrick, A. R. Lewis, S. Margadonna, W. A. Al-Masry, and C. W. Dunnill, *Sci.Rep.*, 7 (2017).
31. Y. Smith, A. Kar, and V. R. Subramanian, *Industrial & Engineering Chemistry Research*, **48**, 10268 (2009).
32. Y. Sohn, Y. Smith, M. Misra, and V. Subramanian, *Applied Catalysis B-Environmental*, **84**, 372 (2008).
33. V. Subramanian, E. E. Wolf, and P. V. Kamat, *J. Phys. Chem. B*, **105**, 11439 (2001).
34. B. Mukherjee, W. Wilson, and V. Subramanian, *Nanoscale*, **5**, 269 (2013).
35. B. Mukherjee, A. Peterson, and V. Subramanian, *Chemical Communication*, **48**, 2415 (2012).
36. L. L. Garza-Tovar, L. M. Torres-Martinez, D. B. Rodriguez, R. Gomez, and G. del Angel, *Journal of Molecular Catalysis a-Chemical*, **247**, 283 (2006).
37. A. Houas, H. Lachheb, M. Ksibi, E. Elaloui, C. Guillard, and J. M. Herrmann, *Applied Catalysis B-Environmental*, **31**, 145 (2001).
38. N. R. deTacconi, J. Carmona, and K. Rajeshwar, *J. Electrochem. Soc.*, **144**, 2486 (1997).
39. K. Rajeshwar, M. E. Osugi, W. Chanmanee, C. R. Chenthamarakshan, M. V. B. Zanoni, P. Kajitvichyanukul, and R. Krishnan-Ayer, *Journal of Photochemistry and Photobiology C-Photochemistry Reviews*, **9**, 171 (2008).
40. A. Watcharenwong, W. Chanmanee, N. R. de Tacconi, C. R. Chenthamarakshan, P. Kajitvichyanukul, and K. Rajeshwar, *J. Electroanal. Chem.*, **612**, 112 (2008).
41. O. M. Ama and O. A. Arotiba, *J. Electroanal. Chem.*, **803**, 157 (2017).